

# Structural Behavior of the Endothelial Glycocalyx Is Associated With Pathophysiologic Status in Septic Mice: An Integrated Approach to Analyzing the Behavior and Function of the Glycocalyx Using Both Electron and Fluorescence Intravital Microscopy

Hanae Kataoka, DDS, PhD,\* Akira Ushiyama, PhD,† Yoshihiro Akimoto, PhD,‡ Sachie Matsubara,§ Hayato Kawakami, PhD,‡ and Takehiko Iijima, DDS, PhD\*

**BACKGROUND:** The endothelial surface layer (ESL) regulates vascular permeability to maintain fluid homeostasis. The glycocalyx (GCX), which has a complex and fragile ultrastructure, is an important component of the ESL. Abnormalities of the GCX have been hypothesized to trigger pathological hyperpermeability. Here, we report an integrated in vivo analysis of the morphological and functional properties of the GCX in a vital organ.

**METHODS:** We examined the behavior of the ESL and GCX, using both electron microscopy (EM) and intravital microscopy (IVM). We also compared morphological changes in the ESL of mouse skin in a glycosidase-treated and control group. Combined approaches were also used to examine both morphology and function in a lipopolysaccharide-induced septic model and the pathophysiological features of leukocyte-endothelial interactions and in vivo vascular permeability.

**RESULTS:** Using IVM, we identified an illuminated part of the ESL as the GCX and confirmed our observation using morphological and biochemical means. In septic mice, we found that the GCX was thinner than in nonseptic controls in both an EM image analysis ( $0.98 \pm 2.08$  nm vs  $70.68 \pm 36.36$  nm,  $P < .001$ ) and an IVM image analysis ( $0.36 \pm 0.15$   $\mu$ m vs  $1.07 \pm 0.39$   $\mu$ m,  $P < .001$ ). Under septic conditions, syndecan-1, a representative core protein of the GCX, was released into the blood serum at a higher rate in septic animals ( $7.33 \pm 3.46$  ng/mL) when compared with controls (below the limit of detection,  $P < .001$ ). Significant increases in leukocyte-endothelial interactions, defined as the numbers of rolling or firm-sticking leukocytes, and molecular hyperpermeability to the interstitium were also observed after GCX shedding in vivo.

**CONCLUSIONS:** Using IVM, we visualized an illuminated part of the ESL layer that was subsequently confirmed as the GCX using EM. Severe sepsis induced morphological degradation of the GCX, accompanied by shedding of the syndecan-1 core protein and an increase in leukocyte-endothelial interactions affecting the vascular permeability. Our in vivo model describes a new approach to deciphering the relationship between structural and functional behaviors of the GCX. (Anesth Analg 2017;XXX:00–00)

Recent studies in intraoperative fluid therapy have focused on preventing postoperative interstitial fluid accumulation<sup>1–3</sup> and individualized intraoperative fluid administration.<sup>4</sup> Such advances are supported by a revised approach to Starling's law<sup>5,6</sup> and a re-evaluation of the "third space" concept.<sup>7,8</sup> According to the revised

Starling's law,<sup>6</sup> extravasation (the outward flow of water from the vessel into the interstitium) should exceed absorption (the inward flow of water from the interstitium into the vessel). Infused fluid thus accumulates in the interstitium and contributes to edema formation.<sup>9</sup> This concept is supported by clinical postoperative outcomes.<sup>10,11</sup>

The interior of the vessel lumen is covered by the glycocalyx (GCX), which plays an important role in forming a tight barrier affecting vascular permeability.<sup>3</sup> The destruction of the fragile GCX in various pathological conditions is thought to enhance fluid extravasation, leading to edema formation and fluid retention.<sup>12</sup> This key component of the regulation of vascular permeability may thus help prevent postoperative fluid retention.

The endothelial surface layer (ESL), including the GCX, is altered in response to surgical stress, anesthesia,<sup>13</sup> and other intraoperative factors.<sup>14</sup> Sepsis and bacteremia may also alter the functional and anatomic state of the GCX.<sup>15</sup> In addition, leukocytes also interact with the ESL. Leukocytes primed during an inflammatory process may adhere to the endothelium, producing microthromboses and inducing microvascular hyperpermeability. In fact, microvascular

From the \*Division of Anesthesiology, Department of Perioperative Medicine, Showa University, School of Dentistry, Tokyo, Japan; †Department of Environmental Health, National Institute of Public Health, Saitama, Japan; and ‡Department of Anatomy and §Laboratory for Electron Microscopy, Kyorin University School of Medicine, Tokyo, Japan.

Accepted for publication February 7, 2017.

Funding: This study was supported by the Japan Society for the Promotion of Science KAKENHI, Grant-in-Aid for Scientific Research (C) 25463145 to T.I.

The authors declare no conflicts of interest.

Supplemental digital content is available for this article. Direct URL citations appear in the printed text and are provided in the HTML and PDF versions of this article on the journal's website ([www.anesthesia-analgesia.org](http://www.anesthesia-analgesia.org)).

Reprints will not be available from the authors.

Address correspondence to Akira Ushiyama, PhD, Department of Environmental Health, National Institute of Public Health, 2-3-6, Minami, Wako, Saitama 351-0197, Japan. Address e-mail to [ushiyama.a.aa@niph.go.jp](mailto:ushiyama.a.aa@niph.go.jp).

Copyright © 2017 International Anesthesia Research Society  
DOI: 10.1213/ANE.0000000000002057

endothelial dysfunction and subsequent end organ failure is now recognized as critical to sepsis pathophysiology.<sup>16</sup>

As the primary interface between circulating blood cells and the vessel endothelium, the GCX acts as a buffer to prevent unnecessary interactions between flowing cells and the endothelium. When an inflammatory process begins, the GCX may become deformed, enabling abnormal interactions to proceed. Although aspects of GCX degradation have been intensively studied, they have not often been correlated with concurrent analysis of the morphological behavior of the GCX.

Since the GCX is less than 500 nm<sup>16</sup> in thickness, most research has utilized electron microscopy (EM) and fixed specimens. The aim of the present study was to combine functional and morphological analysis of the GCX in vivo using EM, intravital microscopy (IVM), and biochemical and physiological measures. We used a mouse dorsal skin-fold chamber (DSC) to allow both observations of GCX behavior and physiological parameters. A lipopolysaccharide (LPS)-induced septic model was used as a pathological model of GCX degradation, and the behavior of the GCX in the face of vascular permeability and leukocyte-endothelial interactions was recorded.

## METHODS

### Animals and Ethical Statement

Experiments were performed using 8- to 10-week-old male BALB/c mice (Japan SLC, Inc, Shizuoka, Japan) weighing 24 to 28 g. The mice were kept in an isolator rack (SuperMouse 1400; Lab Products Inc, Seaford, DE) in a 12-hour light-dark cycle with free access to water and standard chow under controlled temperature (23°C ± 1°C) and humidity (50% ± 10%) conditions.

All experimental protocols were approved by the Committee for Animal Experiments at the National Institute of Public Health (protocol number 26-002) and were in accordance with all the guidelines and laws for animal experiments in Japan.

### Chemicals

Fluorescein isothiocyanate (FITC)-labeled wheat germ agglutinin (WGA) lectin from *Triticum vulgare*, LPS from *Escherichia coli* O26:B6, FITC-labeled dextran (average molecular weight, 40 kDa [FITC-dex40]), tetramethyl rhodamine-labeled dextran (average molecular weight, 75 kDa [TMR-dex75]), hyaluronidase from *Streptomyces hyalurolyticus*, heparinase III from *Flavobacterium heparinum*, lanthanum (III) nitrate hexahydrate, and glutaraldehyde were purchased from Sigma-Aldrich Co (St Louis, MO). Horseradish peroxidase (HRP)-conjugated WGA was purchased from Vector Laboratories, Inc (Burlingame, CA). Ketamine hydrochloride, xylazine hydrochloride, N-acetyl-D-glucosamine (GlcNAc), and rhodamine 6G were purchased from Wako Pure Chemicals Industries, Ltd (Osaka, Japan). Tissue-Tek OCT Compound and 3,3'-diaminobenzidine (DAB) were purchased from Sakura Finetek (Zoeterwoude, the Netherlands) and Nichirei Co (Tokyo, Japan), respectively. The mouse-soluble syndecan-1 (Sdc-1) enzyme-linked immunosorbent assay (ELISA) kit was purchased from Cusabio Biotech Co Ltd (Wuhan, China).

## Identification of ESL

**In Vivo GCX Imaging Using WGA Lectin.** For microvascular observations using the DSC technique, a nonmetal DSC assembly was introduced into each of the recipient mice as previously described.<sup>17</sup> DSC implantation was performed at least 3 days prior to observation to allow surgically induced acute inflammation to subside.

In a pilot study, we tested 7 lectins from various plants to identify a labeling and visualizing the ESL,<sup>18</sup> and FITC-WGA had the most appropriate properties. The FITC-WGA model has been described previously.<sup>18</sup> Briefly, FITC-WGA was solubilized in saline, and a bolus (6.25 mg/kg body weight) was administered via the tail vein 30 minutes prior to imaging. Vascular images within the DSC were observed using an all-in-one epifluorescence microscope (model BZ-9000; Keyence Co, Osaka, Japan) equipped with a high-sensitivity charged-couple device (CCD) camera and a ×20 long working distance objective lens (S PlanFL ELWD ADM 20×C, NA = 0.45; Nikon Co, Tokyo, Japan).

**EM Examination of WGA Lectin Binding.** Male BALB/c mice (n = 6) were deeply anesthetized by the intramuscular injection of a cocktail of ketamine (90 mg/kg body weight) and xylazine (10 mg/kg body weight) and were perfused via the heart using a perfusion pump at a speed of 7 mL/min first with phosphate buffered saline (PBS) and then with 2.5% glutaraldehyde in PBS (35 mL per mouse). After perfusion, the dorsal skin was excised and immersed in 2.5% glutaraldehyde/PBS, and then stored for 24 hours at 4°C. The excised skin was transferred to 10% sucrose/PBS and was allowed to equilibrate for 24 hours at 4°C. This replacement was continued in a stepwise fashion as 15% and 20% sucrose/PBS for 24 hours at 4°C, respectively. The skin was embedded with Tissue-Tek OCT Compound, and sections (thickness, 10 μm) containing small vessels were serially cut in a cryostat (CM1950; Leica Biosystems, Nussloch, Germany). These sections were kept on a Matsunami adhesion slide-coated slide glass (Matsunami Glass Corp, Osaka, Japan) for 3 hours at room temperature, and then reacted with HRP-WGA (8 μg/mL) for 24 hours at 4°C in a moisture box. Sections were stained with chromogen (DAB-H<sub>2</sub>O<sub>2</sub>), washed with PBS, and immersed in 1% glutaraldehyde/PBS. After washing with PBS, the sections were osmicated, and then dehydrated through a graded series of ethanol and embedded in Epon 812 (Shell Chemical Co, New York, NY). Ultrathin sections were cut, slightly stained with lead citrate, and examined using EM (JEM 1011; JEOL, Tokyo, Japan). EM images were obtained using a KeenView III 1k × 1k CCD camera (Olympus Co, Tokyo, Japan). Some sections were incubated with HRP-WGA in the presence of hapten sugar (0.1 M GlcNAc) to confirm WGA staining specificity. Other sections were incubated with DAB-H<sub>2</sub>O<sub>2</sub> solution to detect endogenous peroxidase activity.

### Morphologic Analysis of GCX After Biochemical Digestion With Glycosidase

Animals were divided into 2 groups: a control group (n = 13) and a glycosidase-administration group (n = 13). To confirm that WGA lectin staining was attributable to binding with the hapten sugar (GlcNAc), we compared WGA

staining with or without the intravenous administration of glycosidase (a mixture of hyaluronidase [50 units per mouse] and heparinase [1 sigma unit per mouse]) to mice at 2 hours before observation. Images were obtained using both EM (n = 3) and IVM (n = 10) for each group.

Prior to the IVM observation, a 100- $\mu$ L bolus of FITC-WGA (6.25 mg/kg) for GCX staining and a 100- $\mu$ L bolus of TMR-dex75 (3% w/v) for obtaining blood flow images were injected into the tail vein. Thirty minutes after the lectin and dextran injections, each mouse was anesthetized with 1.5% isoflurane and was mounted on a fluorescence microscope (BZ-9000). Fluorescent images (680  $\times$  512 pixels) were captured for at least 3 regions of interest (ROIs) per chamber using fluorescent filters for FITC and TMR. To compare the fluorescent intensities of the lectin staining, the same exposure time and gain level were used for all the images.

EM was used to examine the arterioles and venules in the dorsal skin. Specimens were prepared from the control group and the glycosidase-administration group (n = 3).

Lanthanum fixation was used because the lanthanum ion ( $\text{La}^{3+}$ ) binds to the negatively charged GCX.<sup>19</sup> Deeply anesthetized mice were perfused via the heart using a perfusion pump for 5 minutes at a speed of 7 mL/min with fixative/staining solution (2% glutaraldehyde, 30 mM (4-(2-hydroxyethyl)-1-piperazineethanesulfonic acid) buffer, and 2%  $\text{La}(\text{NO}_3)_3$ ) after blood removal by perfusion with PBS. Diced pieces of the dorsal skin were immersed in fixative solution (2% glutaraldehyde and 30 mM (4-(2-hydroxyethyl)-1-piperazineethanesulfonic acid) buffer) at 4°C for 24 hours, and then used for EM observations as described above.

### Morphological and Functional Analysis of GCX in LPS-Induced Septic Model

**LPS-Induced Septic Model.** Severe sepsis was induced by the intraperitoneal administration of LPS (2 mg/kg at 0 and 18 hours), according to previous studies.<sup>20,21</sup> To evaluate the sepsis severity, we examined several physiological end points: (1) body weight reduction, (2) decrease in blood pressure, (3) leukocytosis and thrombopenia, (4) decrease in blood albumin level, and (5) 48-hour mortality rates of 40%–50%. The systolic blood pressure and the diastolic blood pressure were measured while the mice were conscious using a computerized tail-cuff system (BA-98A; Softron Co, Tokyo, Japan) at the designated time points. For the biochemical and hematologic analyses, whole blood was collected from the left ventricle of mice at 24 hours and was analyzed using a biochemical analyzer (VetScan VS2; Avaxis Inc, Union City, CA) and a fully automated 5-part differential cell counter (VetScan HM5; Avaxis Inc), respectively.

### Measurement of Sdc-1 Concentrations in Blood Plasma.

The serum level of soluble Sdc-1 was quantified using an ELISA kit according to manufacturer instructions. Briefly, samples, standards, and diluted biotinylated antibody were added to precoated wells and incubated for 1 hour at room temperature. After 3 washes, HRP-streptavidin conjugate was added, and the plate was incubated for 1 hour at room temperature; the substrate was then added, and the color was allowed to develop for 15 to 30 minutes. The absorbance

was read at 450 nm using a microplate reader (Bio-Rad, Hercules, CA). The Sdc-1 concentration was calculated based on a standard curve.

### IVM Examination of ESL and Analysis of Thickness Index.

IVM was performed 24 hours after the first LPS administration. Using the resulting images, the ESL thickness in the LPS and control models (n = 20 from LPS group and n = 10 from control group) was then quantified by transferring the IVM images to BZ image analysis software (Keyence Co). A straight section of endothelium was chosen to measure the thickness. A 2-dimensional graph of the pixel intensities along a line perpendicular to the section was then created. The width of the plot profile at the level of half of the peak was then measured (full width at half maximum). The length was regarded as the ESL length. We defined the mean full width at half maximum as the ESL thickness index (micrometers) for the endothelium.

### EM Examination of GCX and Analysis of Thickness.

For EM observations, perfusion fixation was performed 24 hours after the first LPS administration, similar to the IVM observations. The GCX thickness was measured for the LPS (n = 3) and control (n = 3) groups by transferring the images to the analysis software (ImageJ; NIH, Bethesda, MD). The area of lanthanum staining and the length of the membrane were then measured, and the ratio of these 2 measures (surface area : length) were defined as the mean thickness (nanometers) of the GCX. All analyses were performed in a blinded manner by H.K. and an assistant.

### Observation of Adherent and Rolling Leukocytes Using IVM

The fluorescent marker rhodamine 6G was used to visualize leukocytes in vivo.<sup>17,22</sup> Rhodamine 6G was dissolved in saline at a final concentration of 0.02 mg/mL on the day of the experiment. The solution was filtered through a 0.22- $\mu$ m membrane filter (syringe-driven filter unit, Millex-GN; Millipore Co, Billerica, MA) before each experiment to remove insoluble substances. A prepared rhodamine 6G solution (100  $\mu$ L) was injected into the tail vein at 5 minutes before imaging. During the observation, the animals were anesthetized with isoflurane inhalation and placed on the stage of a fluorescence microscope (BZ-9000). Using a fluorescence filter (excitation, 540 nm; emission, 605 nm; and dichroic mirror, 565 nm), leukocytes were illuminated with rhodamine 6G. We randomly choose an ROI that met the requirements for diameter (about 30  $\mu$ m for arterioles or 40  $\mu$ m for venules) and length (100  $\mu$ m). Flow images were recorded for 30 seconds at a video rate of 30 frames per second for each ROI, and the numbers of rolling and adherent leukocytes were counted. Adherent leukocytes were defined as those that adhered to the endothelium, and rolling leukocytes were defined as white cells moving on the vessel wall at a velocity slower than that of the erythrocytes. The adherent and rolling counts were calibrated for a vascular diameter of 100  $\mu$ m.

### Analysis of Vascular Permeability in IVM

The permeability analysis was performed using a method described by Alfieri et al,<sup>20</sup> with some modifications. Seven

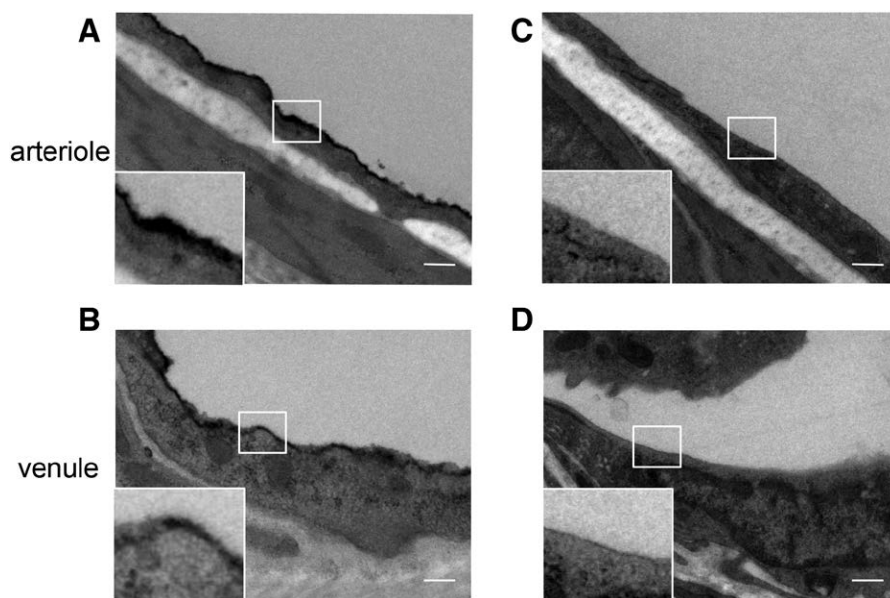


**Figure 1.** WGA lectin binds to the luminal surface of the endothelium. All the specimens were dissected from control mice, and magnified images of arterioles (A and C) and venules (B and D) in subcutaneous tissue are shown. A and B, Specimens stained with HRP-WGA. Positive staining with WGA lectin is shown by the black color. C and D, Specimens without HRP treatment were used as a negative control for HRP-WGA. No staining was identified. The scale bar in each image is 500 nm. HRP indicates horseradish peroxidase; WGA, wheat germ agglutinin.

mice (3 for the septic model and 4 for the control group) were anesthetized with isoflurane inhalation at 24 hours after the first LPS administration. A bolus (200  $\mu$ L) of a cocktail containing 0.5% (w/v) FITC-dex40 and 1.5% (w/v) TMR-dex75 was intravenously injected, and each animal was placed on the stage of a fluorescence microscope (BZ-9000). The microvasculature in the DSC was observed through a  $\times 20$  objective lens, and 5 ROIs per mouse were set using the stage mapping function. Fluorescent images of FITC-dex40 and TMR-dex75 were captured for the same ROI every 30 minutes for up to 120 minutes. To compare the fluorescent intensities, the same exposure time and gain level were used for all images.

Image analysis software (ImageJ) was used for off-line analysis of the fluorescent images. The software assigned an integer value to the brightness of the fluorescence using an arbitrary 8-bit gray scale (range, 0–255) at 3 randomly selected, distinct interstitial areas (900  $\mu$ m<sup>2</sup>) for each ROI. The difference in the value from the first image was used as an index of vascular permeability.

### Statistical Methods

The measured data are presented as the mean  $\pm$  standard deviation. The number of mice used in each experiment is described in the figure legends. Statistical analyses were performed using SPSS statistics software (version 22; Japan IBM Co, Tokyo, Japan). Comparisons were made using an unpaired Student *t* test for the ESL thickness analysis, the GCX thickness analysis, and the analysis of Sdc-1 concentrations. A *P* value of  $<.05$  was considered significant. For leukocyte adhesion, a Mann-Whitney *U* test was used to determine statistical significance. For the permeability analysis, a 1-way analysis of variance followed by a Dunnett post hoc test or a Student *t* test were used as appropriate.

A sample size of 3 for ESL thickness provided more than 90% power at the 0.05 significance level to detect a difference of 0.9  $\mu$ m,<sup>23</sup> assuming a standard deviation of 0.447 (control) and 0.224 (LPS).<sup>23</sup> A sample size of 3 for leukocyte adhesion provided more than 90% power at the 0.05 significance level

to detect a difference of 130/mm<sup>3</sup>,<sup>23</sup> assuming a standard deviation of 0 (control) and 67.08 (LPS).<sup>23</sup>

## RESULTS

### WGA Lectin Bound to the ESL Was Identified Using EM

Images of the HRP-WGA staining (Figure 1) showed the presence of positive staining as a result of peroxidase activity, whereas positive staining of the peroxidase substrate was not observed without HRP-WGA staining. These results suggest that the HRP-WGA–positive component was bound to the luminal surface of the endothelium, within which the glycosaminoglycans (GAGs) of the GCX are thought to be localized.

### Morphological Analysis of GCX Under Biochemical Digestion With Glycosidase

In vivo images of the microvasculature were obtained using IVM (Figure 2A–D). The FITC-WGA lectin signal was present along the luminal surface of the endothelium in control mice (Figure 2A, C), whereas the intravenous administration of glycosidase attenuated the fluorescence signal (Figure 2B, D).

The lanthanum-positive GCX layer and caveola were identified in control mice using EM (Figure 2E, G). In the glycosidase-administration group, degradation of the GCX, which means the layer becomes “thinner,” was also observed (Figure 3C, D). These observations coincided with the IVM results.

### Sepsis Model

In our LPS-based septic mouse model, body weight and survival were monitored for 48 hours. The body weight decreased by approximately 15% in the LPS-administration group, compared with non-LPS controls. A high survival rate (94%) for the first 24 hours was also confirmed. The survival rate at 48 hours after LPS administration was 47.4%. Both systolic blood pressure and diastolic blood pressure decreased with time after LPS administration. These data are shown in Supplemental Digital Content 1, Supplemental Figure, <http://links.lww.com/AA/B714>.

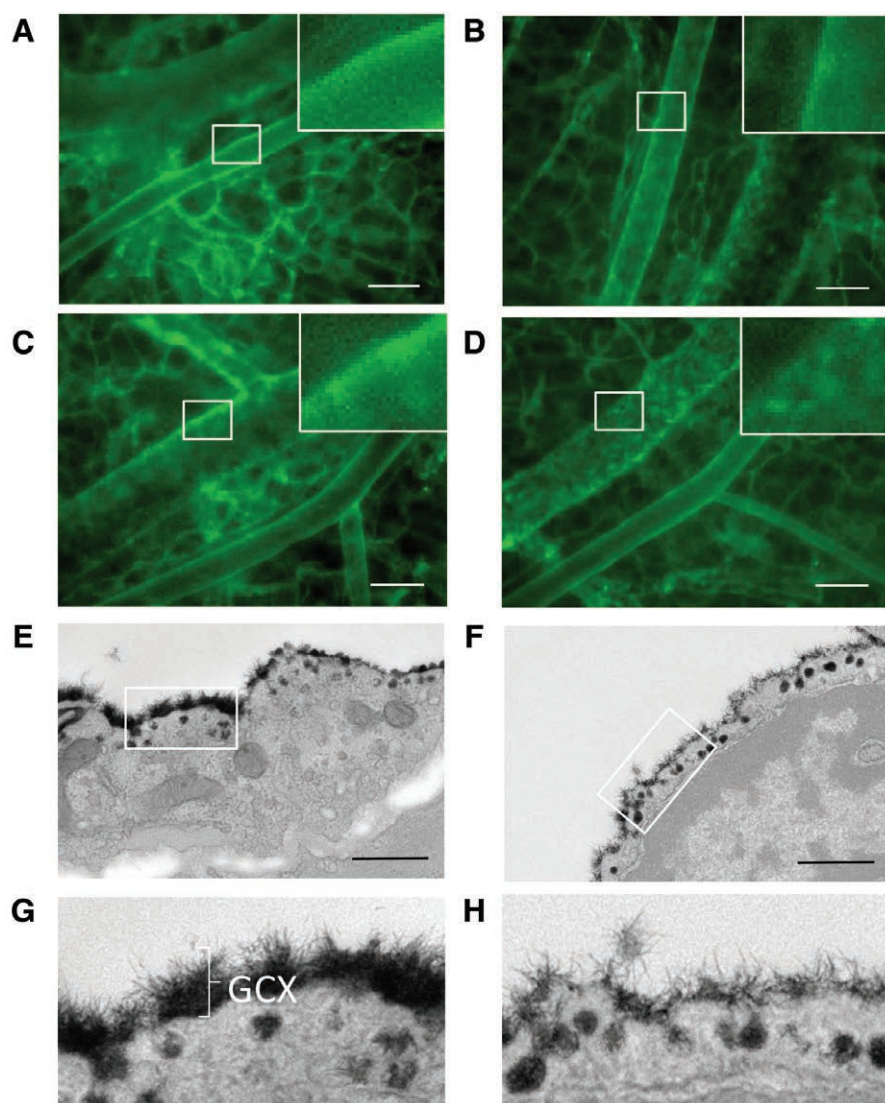


**Figure 2.** Structural stability of GCX is partially affected by glycosidase. A–D, The ESL is weakened by glycosidase when observed using intravital microscopy. FITC-WGA lectin was injected into the tail vein at 30 minutes before observation. The luminal surface of the endothelium was clearly labeled with FITC-WGA in both arterioles (A) and venules (C) in the control mice. In glycosidase-administered mice, the WGA-positive layer signal, which corresponds to the endothelial surface layer, was partially attenuated in both arterioles (B) and venules (D) compared with the signals in control specimens. The scale bar in each figure is 100  $\mu\text{m}$ . E–H, Representative electron microscopic images of subcutaneous venules stained with lanthanum are shown. E and G, Specimens from the control mice are shown. F and H, In glycosidase-treated mice, the lanthanum-positive components were partially eliminated. Images in G and H are magnifications of the rectangles shown in E and F, respectively. The scale bar in E and F is 500 nm. ESL indicates endothelial surface layer; FITC, fluorescein isothiocyanate; GCX, glycocalyx; WGA, wheat germ agglutinin.

Blood samples were collected from the heart under deep anesthesia at 24 hours after the first LPS administration, and white blood cells, platelets, and albumin levels were measured (see Supplemental Digital Content 2, Supplemental Figure, <http://links.lww.com/AA/B715>).

### FITC-WGA Lectin Binding Observed Using IVM and Its Associated Morphological Changes Under Septic Conditions

In vivo images of the vasculature were recorded using IVM (Figure 3). FITC-WGA lectin-positive signals were recognized along the luminal surface of the endothelium in the control mice (Figure 3A, C). However, significantly less binding of FITC-WGA lectin was observed in septic mice (Figure 3B, D). Although the ESL was thinned in both the glycosidase-administered and septic groups, the extent of the decrease in fluorescent intensity and thickness were greater in the septic group than in the glycosidase-administered group. Using these images, we calculated the thickness index of the ESL (Figure 3E). The thickness index in the septic group decreased 70% from the control group.

### Measurement of Sdc-1 Under Septic Conditions

The serum level of soluble Sdc-1 under control and septic conditions was quantified using an ELISA. Under septic conditions, the serum Sdc-1 level was significantly higher than that under control conditions ( $7.33 \pm 3.46 \text{ ng/mL}$  in the septic group versus below the limit of the detection level in the control group; Figure 3F), suggesting shedding of Sdc-1 core protein from the ESL under pathophysiological conditions.

### EM Observations of GCX in Septic Mice

EM images of the capillaries in control mice (Figure 4) revealed a lanthanum-positive GCX layer and caveola (Figure 4A, C). We found that most of the GCX layer disappeared from the endothelium under septic conditions (Figure 4B, D). To quantify the thickness of the GCX in the control and LPS-induced septic mice, we selected postcapillary venules (images not shown) and calculated the thickness using image analysis software. The mean thickness was significantly less in the septic group than in the control group ( $P < .05$ ; Figure 4E).

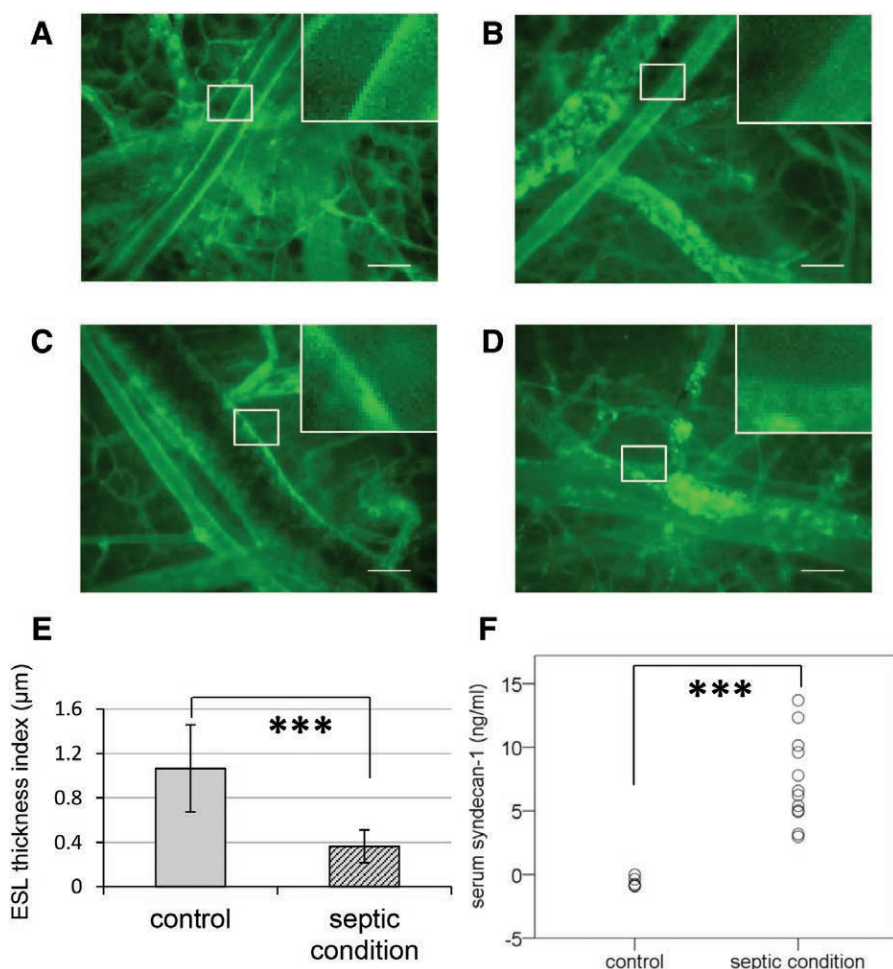


**Figure 3.** Morphologic change analysis of ESL using intravital microscopy and shedding of syndecan-1 into serum in septic mice. The luminal surface of the endothelium was clearly labeled with FITC-WGA in both arterioles (A) and venules (C) in the control mice. In LPS-induced septic mice, both the brightness and the thickness of the FITC-WGA staining in both arterioles (B) and venules (D) were clearly attenuated. The scale bar in each figure is 100 μm. E, A computer-assisted image analysis showed a significant difference in the ESL thickness index between control and septic mice ( $***P < .001$ , unpaired *t* test). F, Significant alterations in serum Sdc-1 in septic mice. Serum was collected at 24 hours after LPS administration. Each plot shows the concentration of soluble syndecan-1 ( $***P < .001$ , unpaired *t* test, *n* = 5 for control; *n* = 12 for septic condition). ESL indicates endothelial surface layer; FITC, fluorescein isothiocyanate; LPS, lipopolysaccharide; Sdc-1, syndecan-1; WGA, wheat germ agglutinin.

### Loss of GCX Under Septic Conditions Induced Leukocyte Adhesion During Subcutaneous Microcirculation

We measured leukocyte adhesion by classifying leukocytes as rolling, adherent, or nonadherent (Figure 5A). In control mice, most of the leukocytes did not interact with the endothelium, although only a few leukocytes adhered to the vessel walls transiently (the so-called rolling). Under septic conditions, however, the number of adherent leukocytes increased significantly, compared with that in the control mice, in both precapillary arterioles (Figure 5B) and postcapillary venules (Figure 5C). Furthermore, some leukocytes tended to adhere firmly to the endothelium under septic conditions. This phenomenon may be attributable to the loss of endothelial GCX and the activation of adhesion molecules on the endothelial surface (see Supplemental Digital Content 3–6, Videos, <http://links.lww.com/AA/B716>, <http://links.lww.com/AA/B717>, <http://links.lww.com/AA/B718>, <http://links.lww.com/AA/B719>).

### Increased Microvascular Permeability Under Septic Conditions

LPS-treated septic mice exhibited significant increases in the fluorescence intensity of FITC-dex40 and TMR-dex75 in nonvascular tissue, compared with control mice, at each time point (Figure 6).

### DISCUSSION

We have demonstrated in a septic mouse model that the morphological attenuation of the endothelial GCX is closely linked to functional changes in vascular permeability. GCX shedding induced by septic conditions led to thinner layer and caused macromolecule hyperpermeability and an increase in leukocyte-endothelial interactions in an in vivo window model. Although this basic study demonstrated real-time degradation of GCX in a septic model, pathological hyperpermeability is an intractable clinical feature of sepsis. Since the pathophysiology of hyperpermeability has not yet been elucidated, we do not have a specific therapeutic strategy for intervening in the pathological vascular leakage of fluid. Therefore, our study demonstrates the feasibility of a model to visualize pathological alterations in vascular permeability.

The endothelial GCX lines the luminal surface of the endothelium and is thought to be an important regulator of endothelial function. The GCX forms a luminal mesh that binds plasma proteins and soluble GAG.<sup>23</sup> The maintenance of a selective endothelial barrier that regulates fluids, proteins, and cellular extravasation is essential for normal organ function.<sup>12,24</sup> However, methodological options for achieving appropriate resolution are limited, and these techniques frequently disrupt the native structure of the GCX. Many studies have used transmission EM to determine the GCX

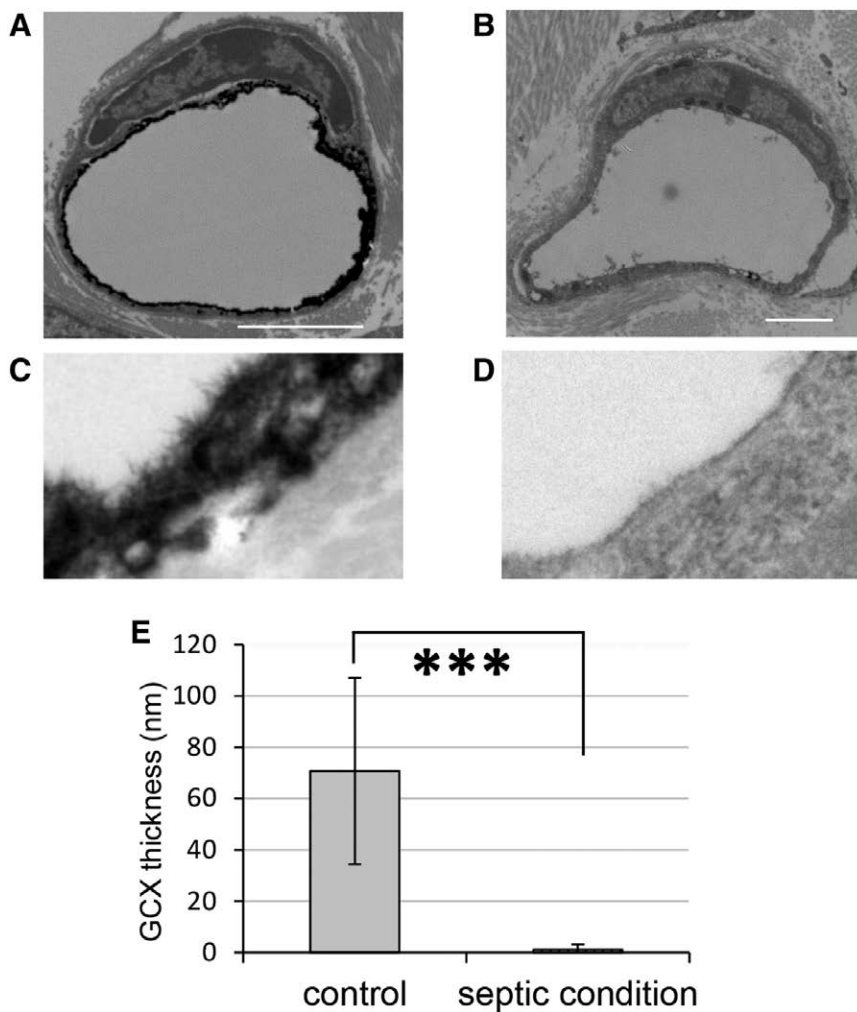


**Figure 4.** Observation of GCX and quantitative analysis of GCX thickness under LPS-induced septic conditions using electron microscopy. Electron microscopy images of cutaneous venules stained with lanthanum are shown. A and C, Specimens from healthy control mice are shown. In LPS-induced septic mice, the lanthanum-positive components were completely eliminated (B and D). The scale bar is 2  $\mu$ m in A and B and 100 nm in C and D. E, The mean thickness of the lanthanum-positive (GCX) layer was significantly different between the control and septic mice. \*\*\* $P < .001$ , unpaired  $t$  test. GCX indicates glycocalyx; LPS, lipopolysaccharide.

thickness,<sup>25,26</sup> whereas IVM studies have mainly focused on GCX pathophysiology, such as molecular permeability.<sup>20,27,28</sup> We were able to confirm the GCX morphology and function simultaneously under both physiological and pathological conditions using EM and IVM.

We used fluorescence-labeled lectin to visualize the GCX and ESL in vivo.<sup>18,29-31</sup> We confirmed that FITC-WGA was the most appropriate lectin for visualizing the ESL in a previous pilot study.<sup>18</sup> In this study, the binding of HRP-WGA to the luminal surface of the endothelium in both arterioles and venules was demonstrated (Figure 1) using EM. To determine whether this binding was specific to WGA lectin, effects of a glycosidase challenge were examined using both EM and IVM. IVM observations showed that glycosidase administration (hyaluronidase and heparanase) weakened FITC-WGA binding to the endothelium, resulting in a partial loss of the ESL (Figure 2). Additionally, EM observations showed that glycosidase partially digested the sugar moieties of GAGs (Figure 2). These results suggest that hyaluronidase and heparanase partly digested polysaccharide chains in the GCX. The overexpression of these enzymes during pathophysiological conditions may thus completely degrade the GCX.<sup>23,32</sup> A systemic inflammatory response to microbial infection may also affect the GCX.<sup>32</sup> Recent clinical studies have shown that the GCX is altered under

septic conditions, and loss of the GCX may predict microcirculatory dysfunction and hypoperfusion.<sup>33</sup> Consistent with previous microscopic observations in glomerular endothelium,<sup>34</sup> LPS-induced sepsis in our study attenuated the staining of the luminal surface of the endothelium by FITC-WGA when observed using IVM, and GCX degradation was observed using EM. This layer was significantly reduced under septic conditions (Figure 4).

The thicknesses estimated using IVM and EM differed from each other. The thicker layer observed using IVM may be attributable to the fact that GAGs in the GCX are enriched with water and soluble proteins, whereas the lanthanum-positive layer observed using EM might reflect a dehydrated condition resulting from specimen preparation. In other tissues, fixation methods that preserve the high water content of the GCX layer resulted in measurements as large as 6  $\mu$ m for rat fat pad and 11  $\mu$ m for bovine aorta.<sup>35</sup> As described above, transmission EM can provide information on the charge, composition, and structure of the GCX; however, results vary greatly, depending on the fixation and staining methods that are used. Therefore, the GCX should be visualized in vital organs to understand its role, function, and biological significance.

Leukocyte adhesion to endothelial cells is complex and involves the capture of free-flowing leukocytes from the

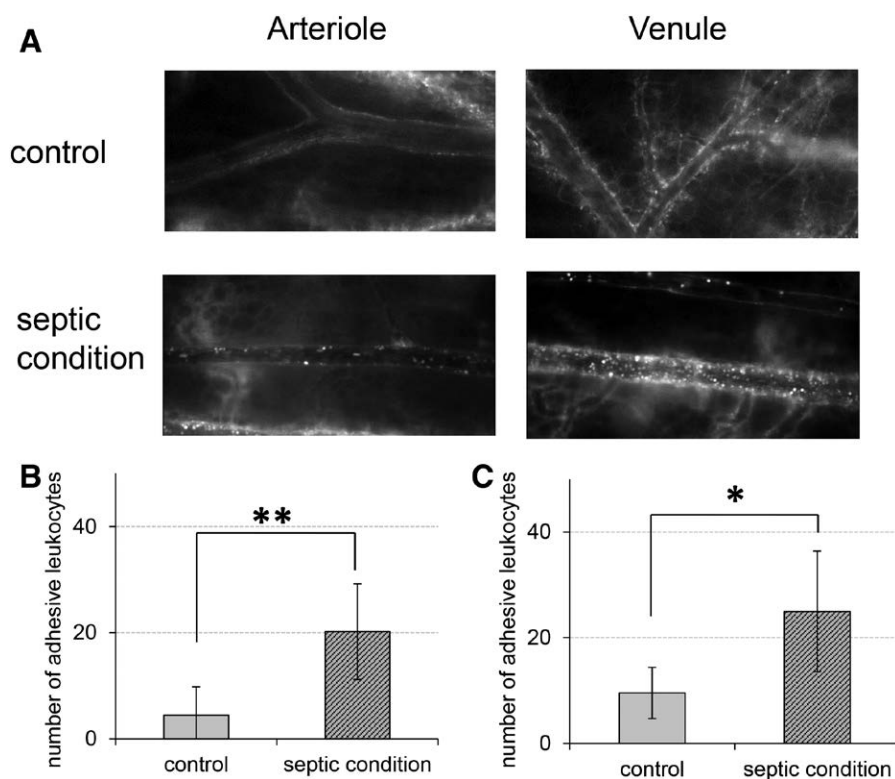


**Figure 5.** Septic conditions increased leukocyte-endothelial interactions in subcutaneous microcirculation. After labeling the leukocytes with rhodamine 6G, intravital fluorescence microscopy was used to visualize the leukocyte-endothelial interactions in septic and control mice. A, Representative fluorescent images of a precapillary arteriole and a postcapillary venule under LPS-induced septic conditions and in control mice. (Movies can be seen in the Supplemental Digital Content 3–6, Videos, <http://links.lww.com/AA/B716>, <http://links.lww.com/AA/B717>, <http://links.lww.com/AA/B718>, <http://links.lww.com/AA/B719>.) The septic conditions increased the number of adherent leukocytes in the precapillary arterioles (B) and postcapillary venules (C) of the subcutaneous tissue. The values are the mean  $\pm$  standard deviation of 4 (control) or 5 (sepsis) mice. \* $P < .05$ , \*\* $P < .01$ , Mann-Whitney  $U$  test. LPS indicates lipopolysaccharide.

bloodstream, rolling on the endothelial surface, deceleration, and eventually, immobilization (firm adhesion). We found that the degradation of the endothelial GCX under septic conditions activated leukocyte-endothelial interactions in not only postcapillary venules but also precapillary arterioles. This finding suggests that the baseline negative charge of the GCX prevents the interaction of leukocytes with the endothelium and adhesion molecules, such as selectins, platelet endothelial cell adhesion molecules, vascular cell adhesion molecules, and intercellular adhesion molecules. These molecules are hidden within the complexed GCX structure under normal conditions but become more accessible during inflammation.<sup>12,36,37</sup> Additionally, adhesion molecules are upregulated under septic conditions.<sup>20</sup>

Hyperpermeability was correlated with septic conditions. In this study, we found that both FITC-dex40 and TMR-dex75 (which has a higher molecular weight) leaked into the interstitium (Figure 6). Similar results in mouse ear skin under inflammatory conditions induced by histamine or immunoglobulin E treatment have also been reported.<sup>38</sup> Although the mechanism is unclear, sepsis increases vascular permeability, allowing albumin to leak into the interstitium and promoting interstitial edema, resulting in hypovolemia.<sup>29,39</sup> In our study, we found both thinning and degradation of the GCX and hyperpermeability, suggesting that the GCX may play a role. The precise role of the GCX in the regulation of water and soluble transport remains unknown. Curry<sup>40</sup> proposed the GCX-junction-break model to explain the function of the GCX: the GCX forms the principal molecular sieve at the vessel wall, which is determined by factors such as the size or number of pores. According to this model, colloid osmotic forces opposing filtration across continuous capillaries develop across the GCX, rather than in the interstitial space, explaining the revised Starling principle.<sup>5,6</sup>

We found another interesting morphology using EM. Lanthanum-positive and caveola-like small vesicles embedded in endothelial cells were identified on EM images obtained in control mice (Figure 2E, G). Similar structures were observed by Wagner et al.<sup>41</sup> Using computer-assisted reconstructions of 3-dimensional tomograms, they found that free vesicles in the endothelial cytoplasm act as transendothelial channels spanning the luminal and lateral membranes. Thus, the caveola-like vesicles shown in Figure 2G might be involved in the regulation of vascular permeability. Further study is needed to determine the function of this structure.

Our study has some limitations. First, the subcutaneous microcirculation examined in this study may not be representative of the changes that occur in other organs during sepsis. Unlike other microcirculation models, the DSC model requires a surgical procedure for chamber attachment, and the possible influence of this surgical procedure on the microcirculation cannot be excluded. Nevertheless, this model has been widely used for studying microcirculation in various studies<sup>20,42</sup> since it enables real-time observations of the microcirculation. Second, we did not measure blood flow in this study; therefore, we could not elucidate how changes in blood flow affect permeability. However, during the observation period, we saw a decrease in blood flow in the sepsis group, compared with that in the control group. Therefore, we should take blood flow into account in future studies to clarify its contribution to changes in permeability. Finally, the use of confocal microscopy would have enabled the thickness of the layer to be measured more precisely because of its improved spatial resolution.

In conclusion, the illuminated area on the ESL observed using IVM was identified as part of the same GCX structure seen by EM. In addition, we demonstrated that GCX

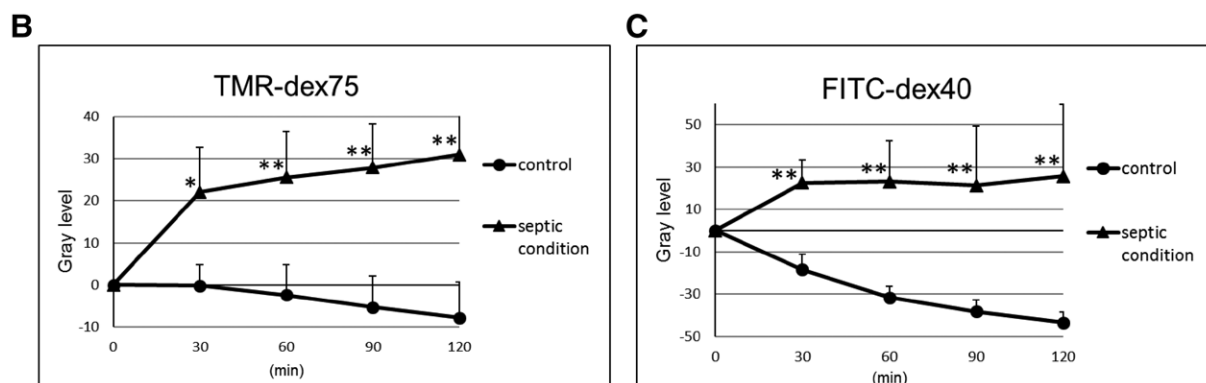
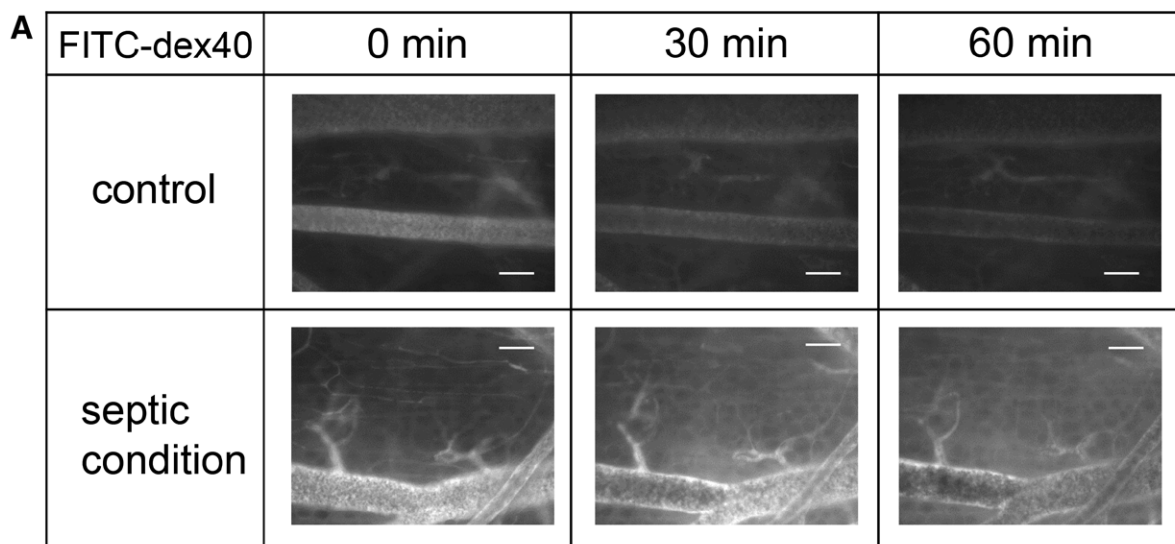


**Figure 6.** Septic conditions triggered vascular hyperpermeability for both FITC-dex40 and TMR-dex75 in septic mice. A, Representative sequential images of both control and septic conditions at 0, 30, and 60 minutes. The elapsed time is shown in the columns. FITC and TMR fluorescence images were obtained for the same region of interest in the DSC. The scale bar in each image is 100  $\mu\text{m}$ . Compared with the control group, the septic group showed an increased vascular permeability. Time-dependent curves in the interstitium for FITC-dex40 (B) and TMR-dex75 (C) are shown. An increase in the fluorescence intensity of the interstitium means vascular hyperpermeability. The permeability of fluorescent dextran was dependent on the molecular size. Data are expressed as the mean  $\pm$  standard deviation of the mean change in the gray level ( $n = 3$  for septic conditions and  $n = 4$  for control). \* $P < .05$ , \*\* $P < .01$  versus control. DSC indicates dorsal skinfold chamber; FITC-dex40, fluorescein isothiocyanate–labeled dextran (average molecular weight, 40 kDa); TMR-dex75, tetramethyl rhodamine–labeled dextran (average molecular weight, 75 kDa).

degradation can be observed in vivo, and that such degradation is closely correlated with leukocyte–endothelial interactions and subsequent hyperpermeability in septic mice. These imaging methods could be applied to various clinical conditions, including sepsis, that are thought to disturb the endothelial microenvironment, including the GCX. Shedding provides a basis for further understanding of the spatiotemporal dynamics of the endothelium and ESL functions. ■■

#### ACKNOWLEDGMENTS

The authors thank Ms Myrna Harrod for her English language review. The authors would also like to thank Mr Yusuke Kan, Ms Yukina Miyasaka, Mr Mao Tanaka, Ms Masako Osawa, Ms Kasumi Yamanaka, Ms Machiko Maeda, and Dr Hideyuki Ochi for their assistance with the experiments and Drs Shin Ohtani, Kohji Uzawa and Hideki Miyao for their expert advice.

#### DISCLOSURES

**Name:** Hanae Kataoka, DDS, PhD.

**Contribution:** This author helped design and perform the experiments, analyze data, and write the manuscript.

**Name:** Akira Ushiyama, PhD.

**Contribution:** This author helped design and perform the experiments, analyze data, and write the manuscript.

**Name:** Yoshihiro Akimoto, PhD.

**Contribution:** This author helped design the experiments and write the manuscript.

**Name:** Sachie Matsubara.

**Contribution:** This author helped perform electron microscopy experiments.

**Name:** Hayato Kawakami, PhD.

**Contribution:** This author helped advise on the concept, and write the manuscript.

**Name:** Takehiko Iijima, DDS, PhD.

**Contribution:** This author helped develop the concept of the experiments, analyze the data, and write the manuscript.

**This manuscript was handled by:** Avery Tung, MD, FCCM.

#### REFERENCES

- Brandstrup B. Fluid therapy for the surgical patient. *Best Pract Res Clin Anaesthesiol.* 2006;20:265–283.
- Wuethrich PY, Burkhard FC, Thalmann GN, Stueber F, Studer UE. Restrictive deferred hydration combined with preemptive norepinephrine infusion during radical cystectomy reduces postoperative complications and hospitalization time: a randomized clinical trial. *Anesthesiology.* 2014;120:365–377.

3. Ushiyama A, Kataoka H, Iijima T. Glycocalyx and its involvement in clinical pathophysiology. *J Intensive Care*. 2016;4:59.
4. Brandstrup B, Svendsen PE, Rasmussen M, et al. Which goal for fluid therapy during colorectal surgery is followed by the best outcome: near-maximal stroke volume or zero fluid balance? *Br J Anaesth*. 2012;109:191–199.
5. Woodcock TE, Woodcock TM. Revised Starling equation and the glycocalyx model of transvascular fluid exchange: an improved paradigm for prescribing intravenous fluid therapy. *Br J Anaesth*. 2012;108:384–394.
6. Levick JR, Michel CC. Microvascular fluid exchange and the revised Starling principle. *Cardiovasc Res*. 2010;87:198–210.
7. Jacob M, Chappell D, Rehm M. The ‘third space’ – fact or fiction? *Best Pract Res Clin Anaesthesiol*. 2009;23:145–157.
8. Iijima T, Brandstrup B, Rodhe P, Andrijauskas A, Svensen CH. The maintenance and monitoring of perioperative blood volume. *Perioper Med (Lond)*. 2013;2:9.
9. Lobo DN, Bostock KA, Neal KR, Perkins AC, Rowlands BJ, Allison SP. Effect of salt and water balance on recovery of gastrointestinal function after elective colonic resection: a randomised controlled trial. *Lancet*. 2002;359:1812–1818.
10. Rehm M, Haller M, Brechtelsbauer H, Akbulut C, Finsterer U. Extra protein loss not caused by surgical bleeding in patients with ovarian cancer. *Acta Anaesthesiol Scand*. 1998;42:39–46.
11. Brandstrup B, Tønnesen H, Beier-Holgersen R, et al; Danish Study Group on Perioperative Fluid Therapy. Effects of intravenous fluid restriction on postoperative complications: comparison of two perioperative fluid regimens: a randomized assessor-blinded multicenter trial. *Ann Surg*. 2003;238:641–648.
12. Bashandy GM. Implications of recent accumulating knowledge about endothelial glycocalyx on anesthetic management. *J Anesth*. 2015;29:269–278.
13. Bruegger D, Brettner F, Rossberg I, et al. Acute degradation of the endothelial glycocalyx in infants undergoing cardiac surgical procedures. *Ann Thorac Surg*. 2015;99:926–931.
14. Bruegger D, Jacob M, Rehm M, et al. Atrial natriuretic peptide induces shedding of endothelial glycocalyx in coronary vascular bed of guinea pig hearts. *Am J Physiol Heart Circ Physiol*. 2005;289:H1993–H1999.
15. Chelazzi C, Villa G, Mancinelli P, De Gaudio AR, Adembri C. Glycocalyx and sepsis-induced alterations in vascular permeability. *Crit Care*. 2015;19:26.
16. Curry FE, Adamson RH. Endothelial glycocalyx: permeability barrier and mechanosensor. *Ann Biomed Eng*. 2012;40:828–839.
17. Ushiyama A, Yamada S, Ohkubo C. Microcirculatory parameters measured in subcutaneous tissue of the mouse using a novel dorsal skinfold chamber. *Microvasc Res*. 2004;68:147–152.
18. Kataoka H, Ushiyama A, Kawakami H, Akimoto Y, Matsubara S, Iijima T. Fluorescent imaging of endothelial glycocalyx layer with wheat germ agglutinin using intravital microscopy. *Microsc Res Tech*. 2016;79:31–37.
19. Chappell D, Jacob M, Paul O, et al. The glycocalyx of the human umbilical vein endothelial cell: an impressive structure ex vivo but not in culture. *Circ Res*. 2009;104:1313–1317.
20. Alfieri A, Watson JJ, Kammerer RA, et al. Angiopoietin-1 variant reduces LPS-induced microvascular dysfunction in a murine model of sepsis. *Crit Care*. 2012;16:R182.
21. Franco-Molina MA, Mendoza-Gamboa E, Castillo-León L, Tamez-Guerra RS, Rodríguez-Padilla C. Bovine dialyzable leukocyte extract protects against LPS-induced, murine endotoxin shock. *Int Immunopharmacol*. 2004;4:1577–1586.
22. Villringer A, Dirnagl U, Them A, Schürer L, Krombach F, Einhäupl KM. Imaging of leukocytes within the rat brain cortex in vivo. *Microvasc Res*. 1991;42:305–315.
23. Schmidt EP, Yang Y, Janssen WJ, et al. The pulmonary endothelial glycocalyx regulates neutrophil adhesion and lung injury during experimental sepsis. *Nat Med*. 2012;18:1217–1223.
24. Steppan J, Hofer S, Funke B, et al. Sepsis and major abdominal surgery lead to flaking of the endothelial glycocalyx. *J Surg Res*. 2011;165:136–141.
25. Jacob M, Bruegger D, Rehm M, et al. The endothelial glycocalyx affords compatibility of Starling’s principle and high cardiac interstitial albumin levels. *Cardiovasc Res*. 2007;73:575–586.
26. van den Berg BM, Vink H, Spaan JA. The endothelial glycocalyx protects against myocardial edema. *Circ Res*. 2003;92:592–594.
27. Torres Filho I, Torres LN, Sondeen JL, Polykratis IA, Dubick MA. In vivo evaluation of venular glycocalyx during hemorrhagic shock in rats using intravital microscopy. *Microvasc Res*. 2013;85:128–133.
28. Landsverk SA, Tsai AG, Cabrales P, Intaglietta M. Impact of enzymatic degradation of the endothelial glycocalyx on vascular permeability in an awake hamster model. *Crit Care Res Pract*. 2012;2012:842545.
29. Salmon AH, Ferguson JK, Burford JL, et al. Loss of the endothelial glycocalyx links albuminuria and vascular dysfunction. *J Am Soc Nephrol*. 2012;23:1339–1350.
30. Tatsuzuki A, Ezaki T, Makino Y, Matsuda Y, Ohta H. Characterization of the sugar chain expression of normal term human placental villi using lectin histochemistry combined with immunohistochemistry. *Arch Histol Cytol*. 2009;72:35–49.
31. Zhou L, El-Deiry WS. Multispectral fluorescence imaging. *J Nucl Med*. 2009;50:1563–1566.
32. Chappell D, Westphal M, Jacob M. The impact of the glycocalyx on microcirculatory oxygen distribution in critical illness. *Curr Opin Anaesthesiol*. 2009;22:155–162.
33. Donati A, Damiani E, Domizi R, et al. Alteration of the sublingual microvascular glycocalyx in critically ill patients. *Microvasc Res*. 2013;90:86–89.
34. Xu C, Chang A, Hack BK, Eadon MT, Alper SL, Cunningham PN. TNF-mediated damage to glomerular endothelium is an important determinant of acute kidney injury in sepsis. *Kidney Int*. 2014;85:72–81.
35. Ebong EE, Macaluso FP, Spray DC, Tarbell JM. Imaging the endothelial glycocalyx in vitro by rapid freezing/freeze substitution transmission electron microscopy. *Arterioscler Thromb Vasc Biol*. 2011;31:1908–1915.
36. Reitsma S, oude Egbrink MG, Vink H, et al. Endothelial glycocalyx structure in the intact carotid artery: a two-photon laser scanning microscopy study. *J Vasc Res*. 2011;48:297–306.
37. Mulivor AW, Lipowsky HH. Role of glycocalyx in leukocyte-endothelial cell adhesion. *Am J Physiol Heart Circ Physiol*. 2002;283:H1282–H1291.
38. Egawa G, Nakamizo S, Natsuaki Y, Doi H, Miyachi Y, Kabashima K. Intravital analysis of vascular permeability in mice using two-photon microscopy. *Sci Rep*. 2013;3:1932.
39. De Gaudio AR, Adembri C, Grechi S, Novelli GP. Microalbuminuria as an early index of impairment of glomerular permeability in postoperative septic patients. *Intensive Care Med*. 2000;26:1364–1368.
40. Curry FR. Microvascular solute and water transport. *Microcirculation*. 2005;12:17–31.
41. Wagner R, Modla S, Hossler F, Czymbek K. Three-dimensional analysis and computer modeling of the capillary endothelial vesicular system with electron tomography. *Microcirculation*. 2012;19:477–484.
42. Miranda ML, Balarini MM, Bouskela E. Dexmedetomidine attenuates the microcirculatory derangements evoked by experimental sepsis. *Anesthesiology*. 2015;122:619–630.